ANNALS OF GEOPHYSICS, 61, 4, PA448, 2018; doi: 10.4401/ag-7457

“APPLICATION OF GROUNDED ELECTRICAL SOURCE AIRBORNE TEM SYSTEM IN CHANGYI BIF DEPOSIT, JIAODONG PENINSULA OF EASTERN CHINA”

Fubo Liu[1,*], Qimao Zhang[1], Zhi Geng[1], Yuxi Pang[1], Yang Li[1], Guangyou Fang[1]

[(1)] Key Laboratory of Electromagnetic Radiation and Sensing Technology, Institute of Electronics, Chinese Academy of Sciences, Beijing, People's Republic of China

Article history
Receveid **June 1, 2017**; accepted November 7, 2017.
Subject classification:
S-ATEM system; Grounded electrical source; Changyi BIF deposit; Underground resistivity distribution.

ABSTRACT

Semi-airborne transient electromagnetic (S-ATEM) method is a hybrid method which employs a grounded electrical or a loop source and an airborne receiver. It has greater investigation depth compared to the airborne electromagnetic method due to its higher transmitting power and more flexibility and efficiency compared to ground electromagnetic method due to its airborne receiving equipment. A new S-ATEM system based on unmanned helicopter is introduced. Besides some information on the technical specifications of the S-ATEM system and data processing technique, a case study of the investigation of Changyi banded iron formation deposit is illustrated. Within the survey area, the ground magnetic method has found a clear magnetic anomaly, whose location has a good correspondence with a ore-body. In order to investigate the underground electrical characteristics and reveal the relationship of ore-body location, subsurface magnetic field anomaly and underground resistivity distribution, a S-ATEM investigation was conducted in January 2016. During the survey, underground resistivity distribution from ground level to a depth of 400 was reconstructed and it was inferred that a strong granite intrusion in the middle of the survey area influenced the ore-body burial depth and magnetic distribution. Although the effect of intrusion on magnetic field is not as significant as that of the ore-body, the intrusion uplifted and deformed the ore-bearing strata, reducing the burial depth and changing the tilt angle, which indirectly affect the magnetic field distribution of the survey area.

1. INTRODUCTION

Electromagnetic (EM) method was considered as an important technique for geophysical exploration. Ground EM method is widely used to achieve underground resistivity investigation however, it is not suitable for low resistivity coverage, strong EM noise, and unreachable regions exploration both in frequency and time domain [Nabighian et al., 2005; Zhdanov et al., 2010]. Transient EM method is characterised by a limited investigation depth in low resistivity coverage area and it is seriously affected by EM noise due to the transmitting power limitation. The audio frequency magneto-telluric (AMT) and controlled-source AMT method has an investigation depth of more than 1 km. However, the high frequency band of AMT and controlled-source AMT is prone to be contaminated by EM noise, this contamination means low resolution in shallow subsurface. In addition, ground EM methods cannot be used in unreachable regions, such as forests, swamps, volcanoes, and deserts.

Airborne EM method has been widely used in geological mapping, environmental engineering, groundwater and geothermal resources, oil and gas and mineral resources exploration over the past few decades [Fountain, 1998]. The mobility of the flying platform makes it suitable for large area exploration.

However, there is a major issue that limits the airborne EM system, i.e. the investigation depth. To achieve deep investigations, a new type of airborne system with ground-based transmitter and airborne receiver was introduced in 1970s [Bosschart et al., 1972]. Semi-airborne transient EM (S-ATEM) is a hybrid method which employs a grounded electrical source or a fixed-loop source for large transmitting power and an airborne receiving for flexibility and efficiency. It was further developed by Elliott [1996] and Mogi et al. [1998] with fixed-loop source and grounded electrical source, respectively. The S-ATEM system has been used for metal mineral exploration in arid area [Elliott, 1998], unreachable crater structure investigation [Mogi et al., 2009; Ito et al., 2014], coastal or shallow sea areas underground structure investigation [Ito et al., 2011; Abd Allah et al., 2013; Abd Allah et al., 2014], rugged terrain tunnel construction design [Okazaki et al., 2011], and achieved good survey results.

A comparison of the data from airborne, semi-airborne, and ground EM systems was done by Smith et al. [2001]. They summarized that semi-airborne system is more efficient than ground system due to the airborne receiver and has a higher signal-to-noise ratio compared to the airborne system due to the higher transmitting power.

In this paper, a new S-ATEM system based on unmanned helicopter system (UHS) is introduced, this system employs a grounded electrical source and with a lightweight design of the acquisition system. A case study in Changyi banded iron formation (BIF) deposit is also shown including the survey information and data analysis. We describe the characteristics of the regional geology, BIF deposit, lithology, and magnetic field in the survey area. We also delineate the geo-electrical structure and ore-body distribution of the survey area by combining the S-ATEM result with prior geo-information.

2. METHODOLOGY

2.1 S-ATEM SYSTEM

Figure 1 is an overview of the S-ATEM system, it consists of a transmitter unit, a receiver unit, and an aircraft. The transmitter unit and receiver unit are developed by the Institute of Electronics Chinese Academy of Sciences and the primary technical parameters are listed in Table 1.

The maximum transmitting power is up to 20 kW, it is dangerous to work near the launch system. Taking into account the safety of the operator, a controller box was used to control the launch system 10 meters away. The basic frequency and duty cycle are adjustable according to the expected investigation depth. The receiver unit includes multi-channel recorder, three-component sensor and inertial navigation system (INS). Multi-channel recorder is installed in the UHS cabin with 24 bit ADC (Analog-to-Digital Converter). A dual-gain collection technique is used for large dynamic signal acquisition, low-gain channel is used in the vicinity of the source to prevent signal saturation while high-gain channel is used far from the source to improve the signal strength.

A new orthogonal three-component induction coil sensor is designed with the characteristic of larger effective area, higher resonant frequency and lower noise level for greater investigation depth. The coils are installed in the bird suspended about 25 m below the UHS. The coordinate and attitude information of the bird is recorded by INS with coordinate accuracy less than 1 m and attitude dynamic accuracy less than 0.1 degree.

An UHS with an admissible payload of more than 80 kg was used as aircraft to take into consideration system weight and flight safety.

2.2 DATA PROCESSING

Figure 2 schematically displays S-ATEM system data processing technique. The raw data include airborne EM data, current waveform data, bird coordinate and attitude data, and ground-base GPS data. The current waveform data is used for system response correction and ground-base GPS data is used to improve the bird coordinate precision. The airborne EM data processing technique include sferics noise removal, motion-induced noise suppression, coil attitude correction, stacking and filtering, and one-dimensional inversion.

1) Sferics noise removal

Sferics are EM radiations caused by lightning strokes. In some circumstances, sferics are a significant source of random noise in airborne transient EM systems [Buselli et al., 1996]. A sferics noise pruning technique was introduced by Macnae et al. [1984]. The recorded signal contaminated by sferics above a fived threshold level is replaced with a smooth response obtained by interpolation within the time window of the edited data. In their opinion, signals which are contaminated by large amplitude sferics noise totally should be rejected rather than added to stack.

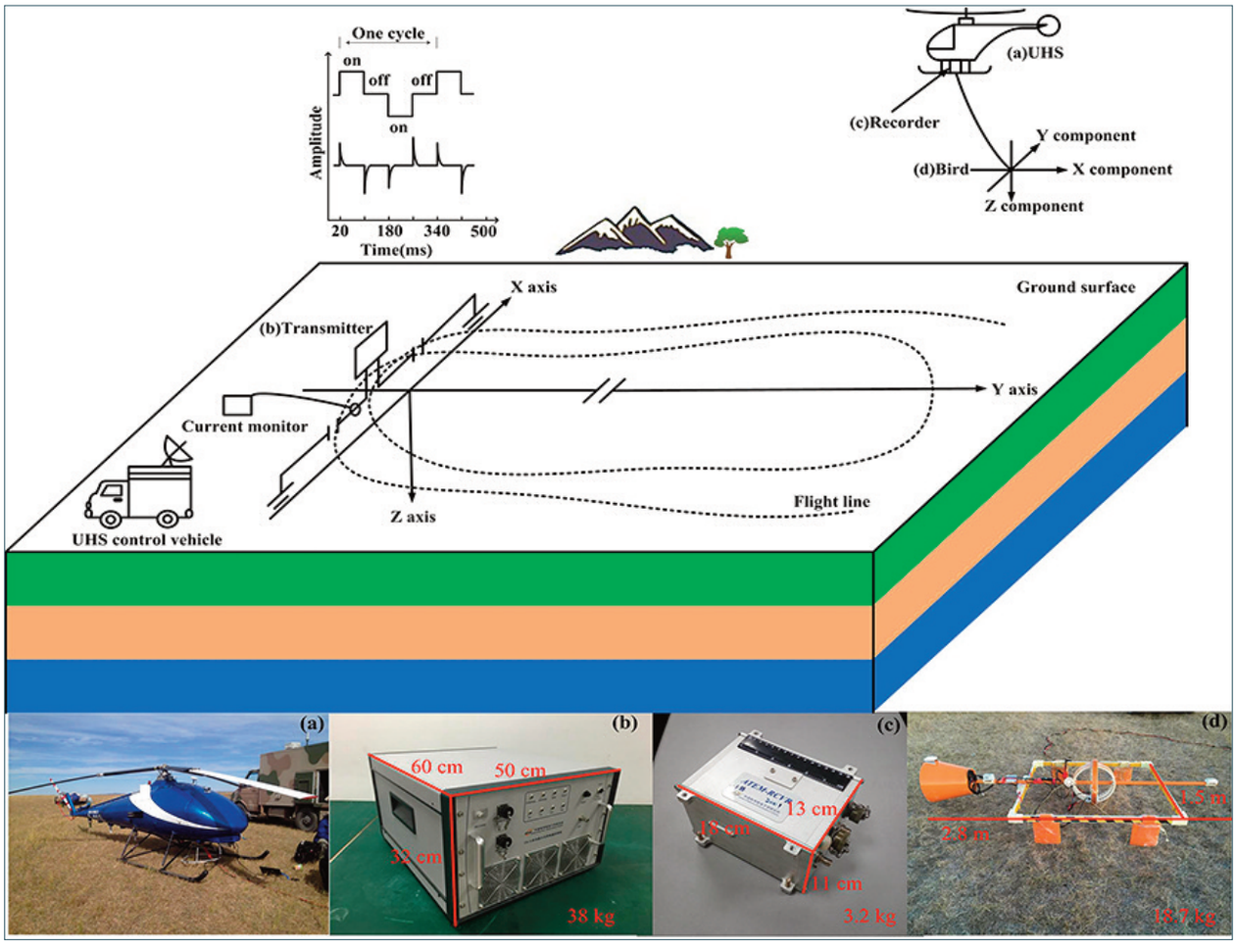

FIGURE 1. Design of the S-ATEM system. (a) UHS, (b) transmitter, (c) recorder, (d) bird.

Transmitter		Receiver	
Source type	Grounded electrical source	Coils	Standard Z, optional X, Y
Pulse shape	Bipolar square waveform	Coils shape	Z (square), X and Y (Circle)
Base frequency	12.5 Hz (typically), 6.25 Hz	Effective area	Z (24000 m^2), X and Y (5700 m^2)
Maximum power	20 kW	Sample rate	48 kHz over entire waveform
Current duty	Adjustable (typically 50%)	Band width	20 kHz
Sync and accuracy	GPS (100 ns)	Coils noise level	Z (0.5 nT/s), X and Y (1.4 nT/s)
Current monitor	Yes, 0.5 A resolution	Terrain clearance	50m ~ 100m

TABLE 1. Primary technical parameters of S-ATEM system.

2) Motion-induced noise suppression

Motion-induced noise exists in any form of moving EM system [Munkholm, 1997] with the main energy concentrated in low frequency band [Lane et al., 2000]. A new motion-induced noise distinction and suppression method has been introduced by Liu et al. [2017] using ensemble empirical mode decomposition method. Signals are decomposed into N intrinsic mode functions (IMFs) and a residual function. Separation of low frequency IMF components which contain the motion-induced noise, from the noise-free signal can be obtained by

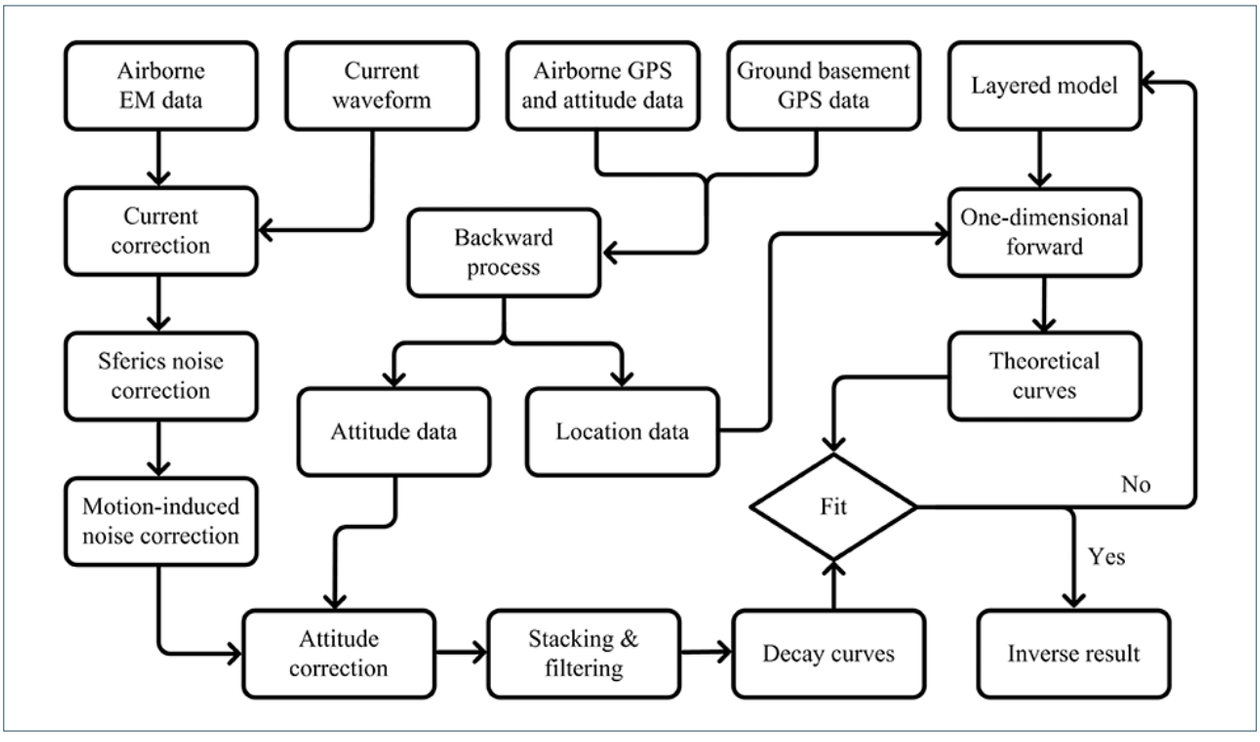

FIGURE 2. Overview of S-ATEM system data processing technique.

reconstruction with the obtained IMFs and residual function.

3) *Attitude correction*

The attitude and coordinate data are recorded by INS for attitude correction and inversion. Attitude data include yaw, pitch, and roll representing bird angles variation in three directions. An improved rotation matrix was used for attitude correction based on Yin et al. [2004] and Fitterman et al. [2004]. The rotation matrix retains only the receiving coils correction for S-ATEM system.

4) *Stacking and filtering*

Data stacking and filtering is used to minimize the random noise and antropic noise. The flight speed of UHS is about 54km/hr, for typical basic operating frequency of 12.5 Hz, we can get a lateral resolution up to 15 m and stacking cycles up to 25 times when taking a time interval of 1 s. It may be more effective to use 2-second intervals in noisy regions. A median filter is used to smooth the decay curves after stacking.

5) *One-dimensional inversion*

One-dimensional Occam's inversion based on smooth model is used for field data inversion [Constable et al., 1987], the subsurface structure can be obtained by comparing the field curve to the theoretical curve. The coordinate data X, Y and Z (representing the distance in three directions from the receiving point to midpoint of the source) from INS are used in forward modelling due to transmitter-receiver geometry variation.

3. SURVEY AREA

3.1 REGIONAL GEOLOGY

The survey area is located in Laizhou-Anqiu iron ore belt, northeast of Jiaodong Peninsula [Song, 2008]. The main strata are the Paleoproterozoic Fenzishan Group and Jingshan Group (see Figure 3). Laizhou-Anqiu iron ore belt is located in NNE direction and extends for about 100 km from north to south. There are more than 20 iron deposits distributed in this belt that can be divided into three types: magmatic hydrothermal iron deposit, deposition metamorphic iron deposit and magmatic differential iron deposit [Wang et al., 2007; Wang et al., 2014].

Changyi BIF deposit is located in the middle of Laizhou-Anqiu iron ore belt in the NE direction. The orebody appeared in a layered- or lens-like from in surrounding rock. The surrounding rock is mainly composed of metamorphic rocks, and the lithology varies in a wide range. It can be divided into acidic plagioclase gneiss and petrolites, garnet-bearing schist and gneiss, medium and basic amphibolite and plagioclase amphibolites. The bottom of the metamorphic rock is intruded by granite in different depths [Lan et al., 2012].

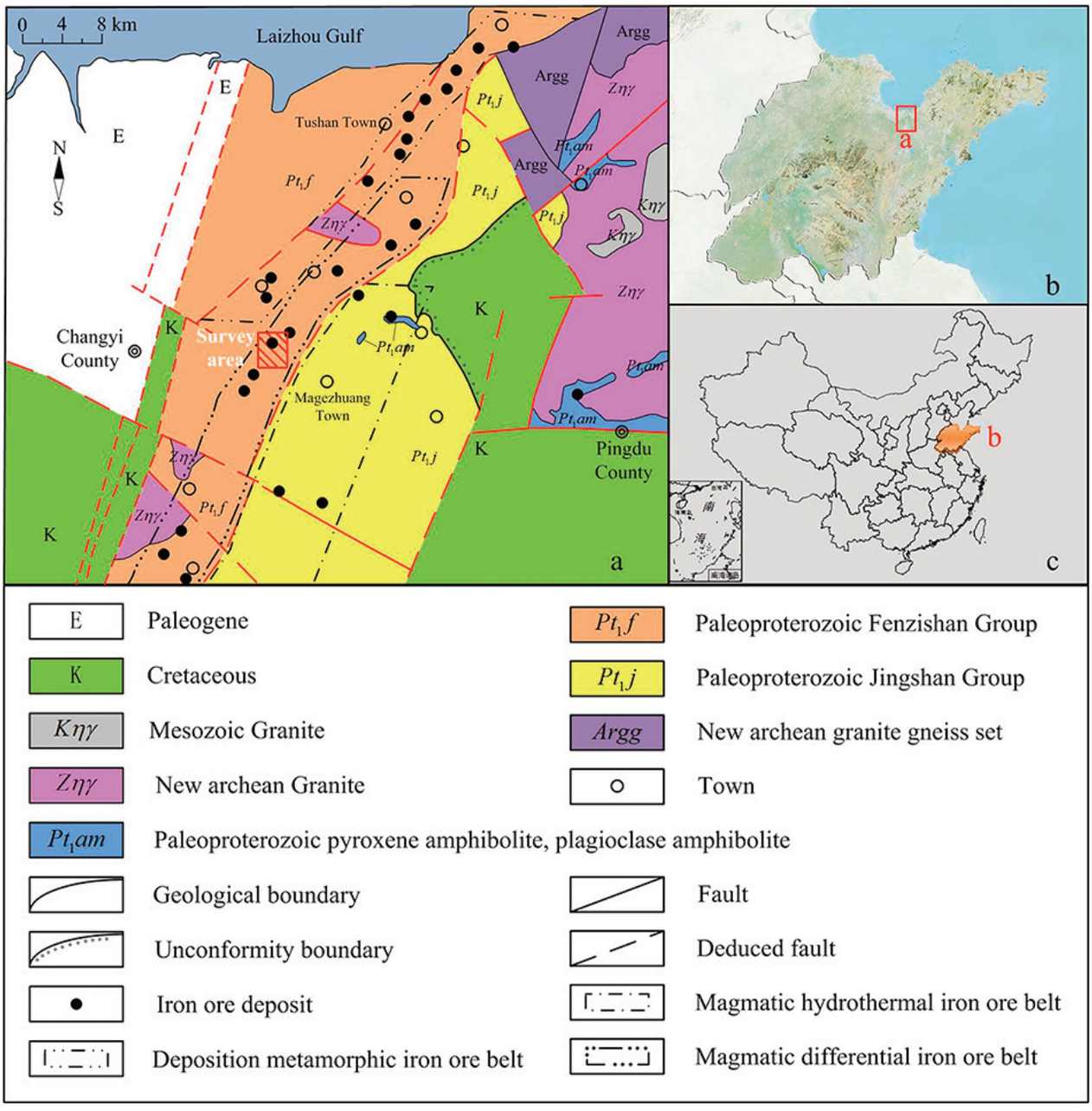

FIGURE 3. Regional geology map of Laizhou-Anqiu iron ore belt and survey area location [after Wang et al., 2007].

3.2 BIF DEPOSIT

Changyi BIF deposit is formed in a marine sedimentary environment. The ferromagnetic minerals in magma aggregate through the volcanic extrusion and the seawater differentiation procedure. The layer- or lens-like BIF orebody formed in the bedrock through the deposition, extrusion, and metamorphism. Zeng et al. [1998] proposed that the component of Changyi iron deposit is related to basic and mid-acid volcanic eruption of the seabed. Iron in mantle-derived substance is brought into seawater by volcanic eruption and then decomposed to silica gel which formed the iron deposit after sedimentation and metamorphism. Lan et al. [2012] agree with this opinion and further studied the formation of Changyi iron deposit. They pointed out that Changyi iron deposit occurs in metamorphic rocks of Paleoproterozoic Fenzishan Group with stripe-like formation which has the typical characteristics of BIF deposit.

Figure 4a shows a borehole profile performed in survey area. The earth's surface is covered by Quaternary Linyi Group with thickness from 20 m to 60 m. Following is the Paleoproterozoic Fenzishan Group and the lithology is biotite granulite or biotite granulite with garnet. The orebody is distributed in metamorphic rocks, and the depth

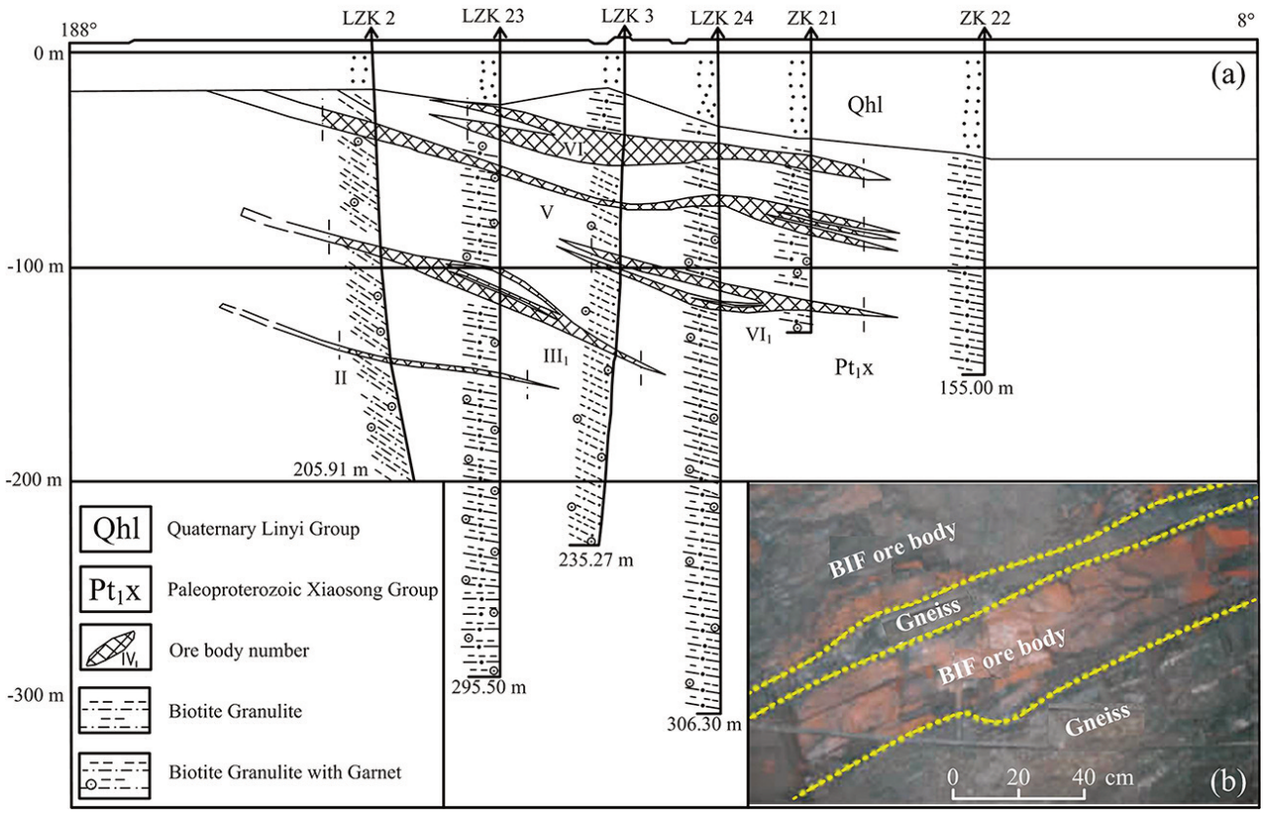

FIGURE 4. A borehole profile in survey area and a typical BIF ore-body from downhole. [after Wang et al., 2014 and Lan et al., 2012].

of the ore-body is less than 200 m. There are granite intrusions at the bottom of the metamorphic rocks in some regions which cannot be seen in this profile. Figure 4b is the picture of a typical BIF ore-body from a downhole. The BIF ore-body is layered-like distribution in the gneiss.

3.3 LITHOLOGICAL FEATURES

The physical properties of the rock samples, coming from boreholes (whose location is shown in Figure 6a), have been measured in laboratory. Table 2 lists the resistivity, magnetic susceptibility, and density of nine major rocks in survey area. Most of rocks in this area have a resistivity in the range of 100 Ωm - 1000 Ωm. Chlorite schist has a resistivity less than 100 Ωm due to fracture or porosity filled with underground water. Granite from deep intrusion has a resistivity of more than 10000 Ωm without weathering. The magnetic susceptibility difference between the magnetite and non-magnetite is noticeable. The rock density difference is not obvious, while the density of magnetite is slightly larger.

3.4 MAGNETIC FEATURES

Figure 5 displays the total magnetic field distribution over the survey area. Magnetic data have been collected by ground total magnetic field measurement. The magnetic field appears a stripe-like in east-west direction with low magnetic field in northern side and high magnetic field in southern side in general.

There are three closed magnetic anomalies in the middle of the survey area, including two positive anomalies M1 and M2 and a negative anomaly M3. Considering that the value of the Earth's magnetic field in this area is of 52121 nT, from Figure 5 it follows that the amplitude of the anomalies is approximately in the interval -500 nT to +500 nT. There is an unclosed magnetic anomaly (M4) with magnetic amplitude slightly positive in the eastern part of the survey area. Projecting the existing geological and borehole data [Wang et al., 2014] on the magnetic contour map it is possible to determine that the magnetic anomaly M1 and M2 is due to underground orebody, although we do not know the distribution and formation of the ore-body exactly. Another finding is that the M1 and M2 anomalies may have been a complete magnetic anomaly until the appearance of F1 fault.

The negative anomaly M3 is related to the absence of ferromagnetic material underground. There is no evidence to make hypothesis on the formation of M4 anomaly.

Sample number	Lithology	Resistivity (Ωm)	Magnetic susceptibility (10^{-3}SI)	Density (g/cm^3)
N1	Granite	16322	0.65	2.604
N2	Granite with weathering and porosity	907	5.96	2.600
N3	Magnetite	445	874.50	3.489
N4	Gneiss	460	0.44	3.011
N5	Schist with biotite and fracture	309	1.98	3.149
N6	Mica schist with fracture	444	0.06	2.760
N7	Garnet biotite schist with fracture	560	0.75	3.092
N8	Chlorite schist with fracture and porosity	37	0.32	2.641
N9	Sandstone	103	0.155	2.563

TABLE 2. Lithological characteristics of Changyi BIF deposit.

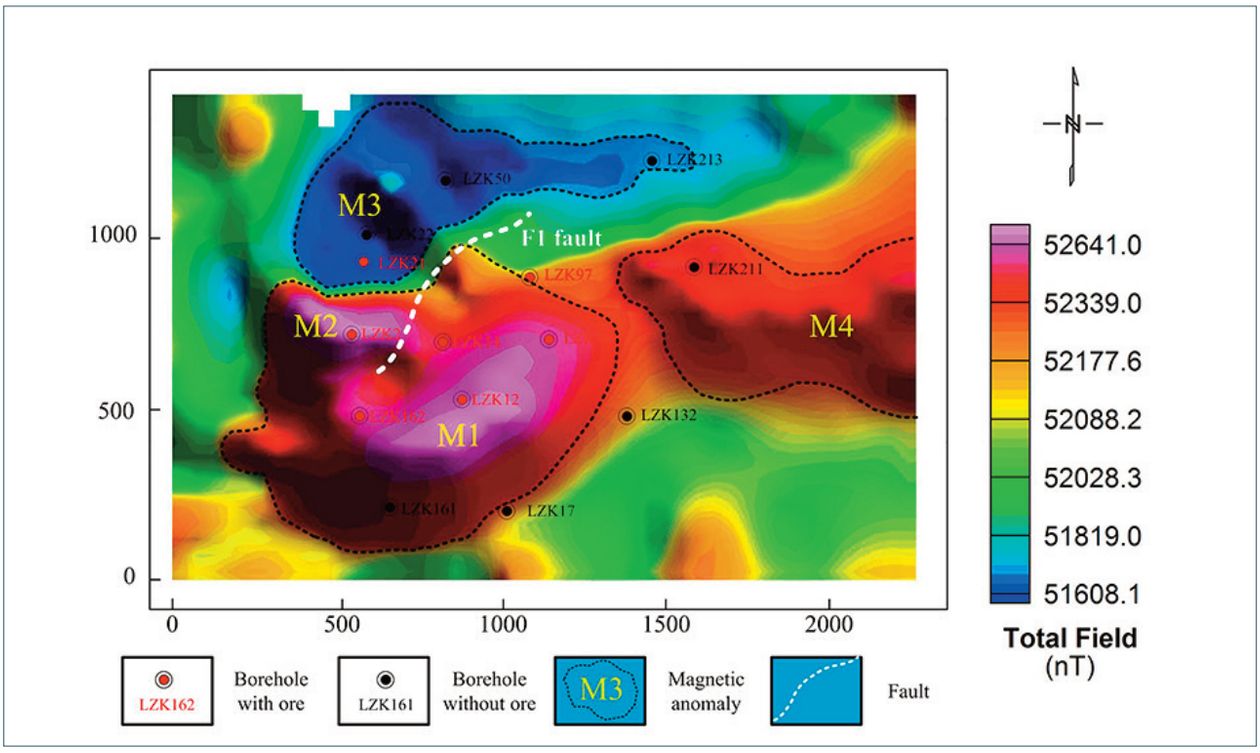

FIGURE 5. Magnetic characteristic of the survey area.

4. FIELD SURVEY

In January 2016, a S-ATEM field survey was carried out in Changyi BIF deposit for underground resistivity investigation. A grounded electrical source (white solid line in Figure 6a) with a length of 2.77 km was deployed along a road with east-west direction. The wire source is about 400 m from the magnetic measurement area (yellow rectangle with dotted line in Figure 6a). The data near the wire source are discarded since the Z component transient response in places close to the source is attenuated rapidly to amplitudes less than noise level. The depth of investigation decreased even though the

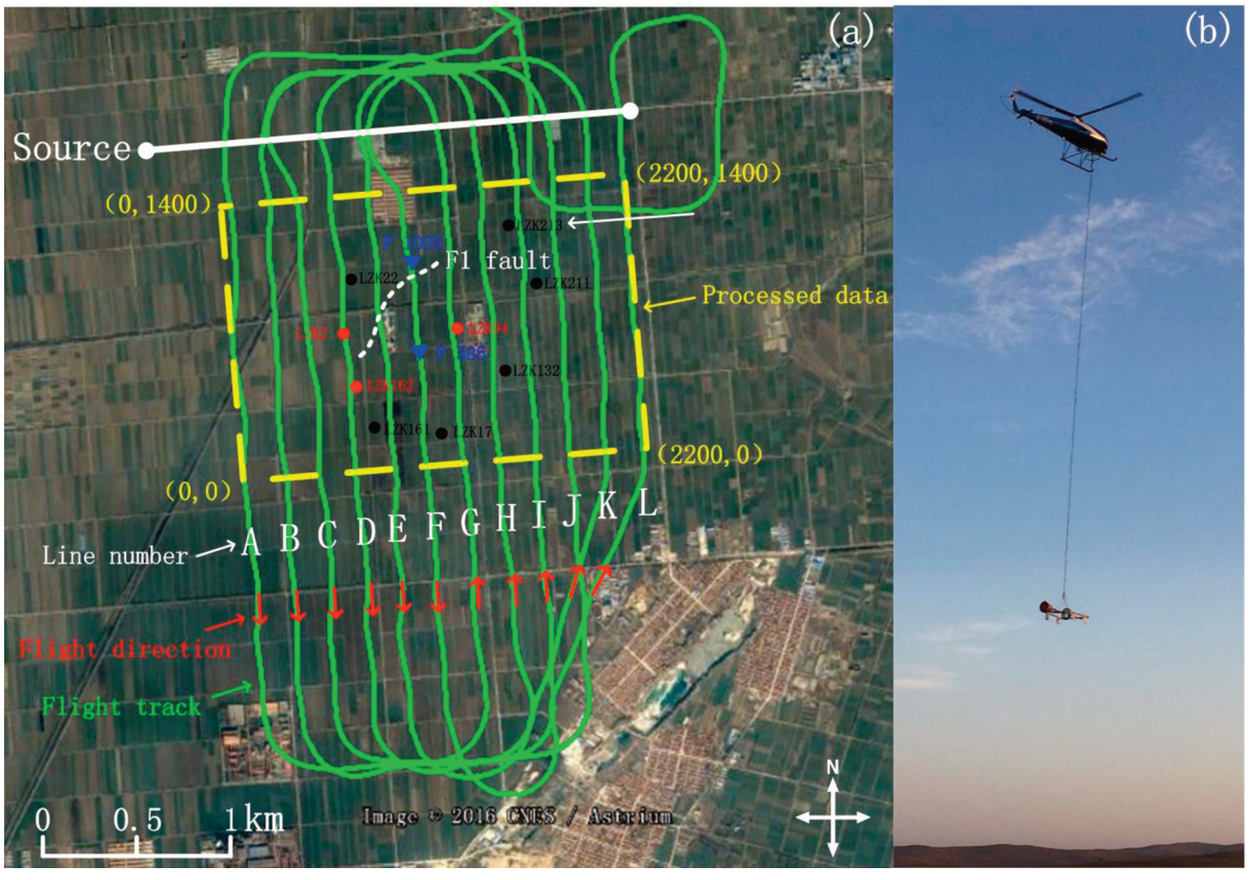

FIGURE 6. Flight details concerning of Changyi BIF deposit investigation. The red/black dots represent part of boreholes with/without ore. The blue triangles represent the location of the decay curves shown in Figure 7.

initial signal strength is high [Mogi et al., 2009]. The used transmit current is of 25 A and the basic frequency of 12.5 Hz. The waveform is a bipolar square waveform with 50% duty cycle. The flight track (green solid line in Figure 6a) is perpendicular to the source and characterised by a spacing of 200 m. The line number and flight direction are also shown in Figure 6a with white letters and red arrows, respectively. A picture took during a flight performing S-ATEM measurements is shown in Figure 6b, the flight speed was about 54 km/hr and the average height of the coil to the ground is 90 m. For ease of explanation, the same rectangular

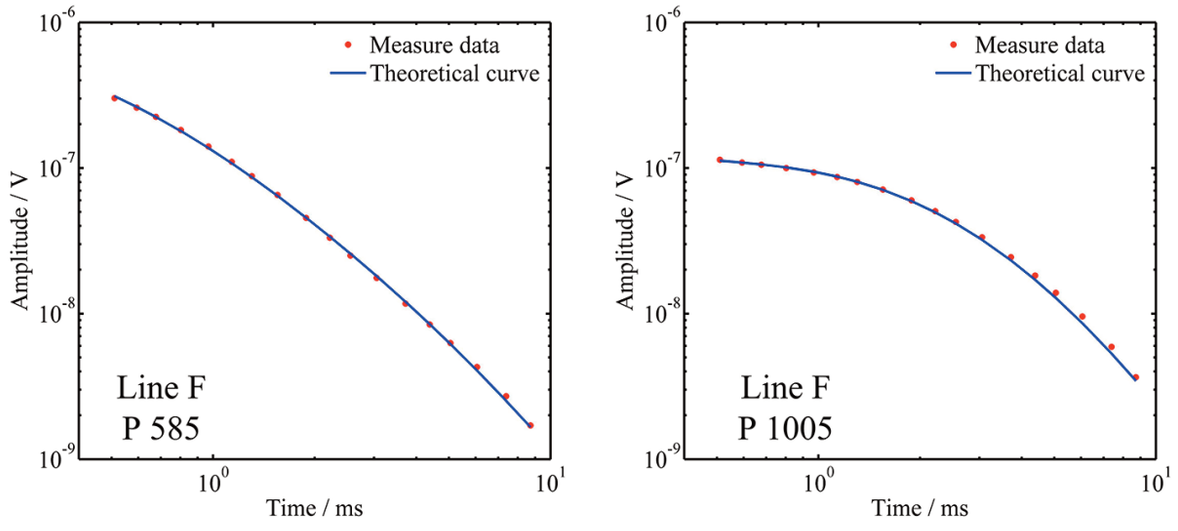

FIGURE 7. Typical decay curves of the Z component after pre-processing and inversion result (amplitude normalized by transmitting current and coil area).

area where ground magnetic method was performed, was selected for data processing. While using the same coordinate system, measurement point number increased from south to north and line number increased from west to east regardless of flight number and direction.

To suppress the strong anthropic noise, 2-second interval data are superimposed to get one measurement point corresponding to lateral resolution of about 30 m. Figure 7 shows two typical decay curves of the Z component which represent the response of different receiving positions and resistivity stratifications. The curves are smooth after pre-processing and the ideal inversion result can be obtained as shown by the good fit of field data and theoretical data.

5. DATA ANALYSIS

Figure 8 displays the one-dimensional resistivity profile of line D; red colour represents low resistivity and blue colour represents high resistivity: three main layers can be identified from ground level to a depth of 400m. The first layer is Quaternary with the resistivity ranging from several to several tens Ωm, and depth from ten meters to tens of meters. The second layer is mainly the Paleoproterozoic Xiao-song Group metamorphic rocks with the resistivity ranging from dozens to hundreds Ωm, which is the main deposit stratum of ore-body. The third layer resistivity ranges from more than several hundred Ωm to even more than 1000 Ωm due to the granite base.

Projecting the boreholes and ore-body onto the resistivity profile according to the position shown in Figure 6a, we can suggest the following interpretation. The ore-body distributed in Quaternary and Paleoproterozoic Xiao-song Group metamorphic rocks, and the tilt angle of the ore-body is consistent with the resistivity distribution. We inferred that the high resistance tongue around 700 m could be due to the granite branches intrusion according to the lithological characteristics of the survey area. Due to the intrusion, the ore-body and the strata overlaid to the ore-body are broken and tilted, which lead to the positive and negative magnetic anomaly at the ground surface. From the profile shown in Figure 8, it can be inferred that the ore-body at distances between 400 m and 700 m is characterised by the same tilt observed at distances between 700 m and 1000 m, of course with the opposite angle of inclination.

Figure 9 displays the one-dimensional resistivity profile of line F, which shows that line F has a greater range of intrusion from 400 m - 950 m if compared to line D. In this profile it is possible to observe a typical geological structure, i.e. a fault (F1), that is present in the surveyed area passing through line F at a distance of about 1000 m (see details in Figure 6a). This fault is clearly shown in the resistivity profile of Figure 9 with accurate position and inclination. The blue triangles represent the position where the measurements of the decay curves shown in Figure 7 have been made.

Figure 10 represents the resistivity slice map at a depth of 200 m which delineates the resistivity distribution of the survey area in general. In order to analyse comprehensively the relationship among the different data shown so far, magnetic anomaly, boreholes, and fault location are superimposed to the slice map. The abundant geo-information mentioned above can help us to understand the conformation and distribution of the BIF deposit.

The ore-body is distributed in high positive and negative magnetic anomaly M1, M2, and M3 with its main part in the positive magnetic anomaly according to

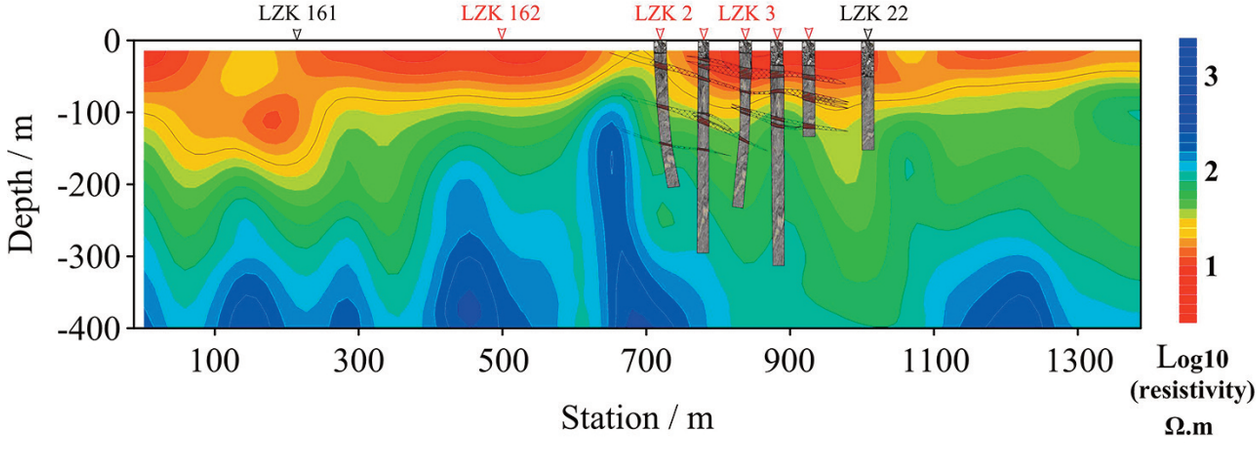

FIGURE 8. One-dimensional resistivity profile of line D. The red/black arrows represent boreholes with/without ore in this profile. The horizontal axis displays the distance of the profile from the southern border of the yellow dotted rectangle show in Figure 6.

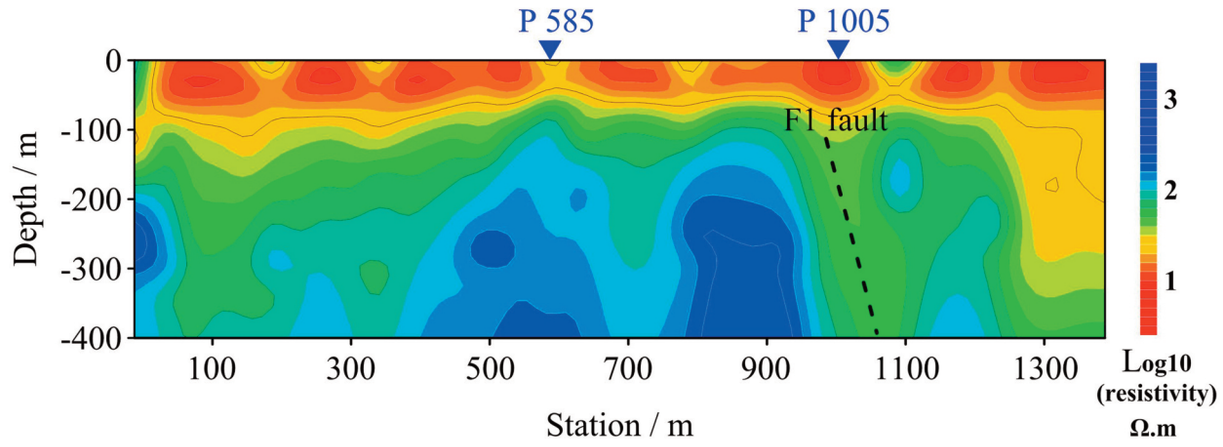

FIGURE 9. One-dimensional resistivity profile of line F. The horizontal axis displays the distance of the profile from the southern border of the yellow dotted rectangle shown in Figure 6.

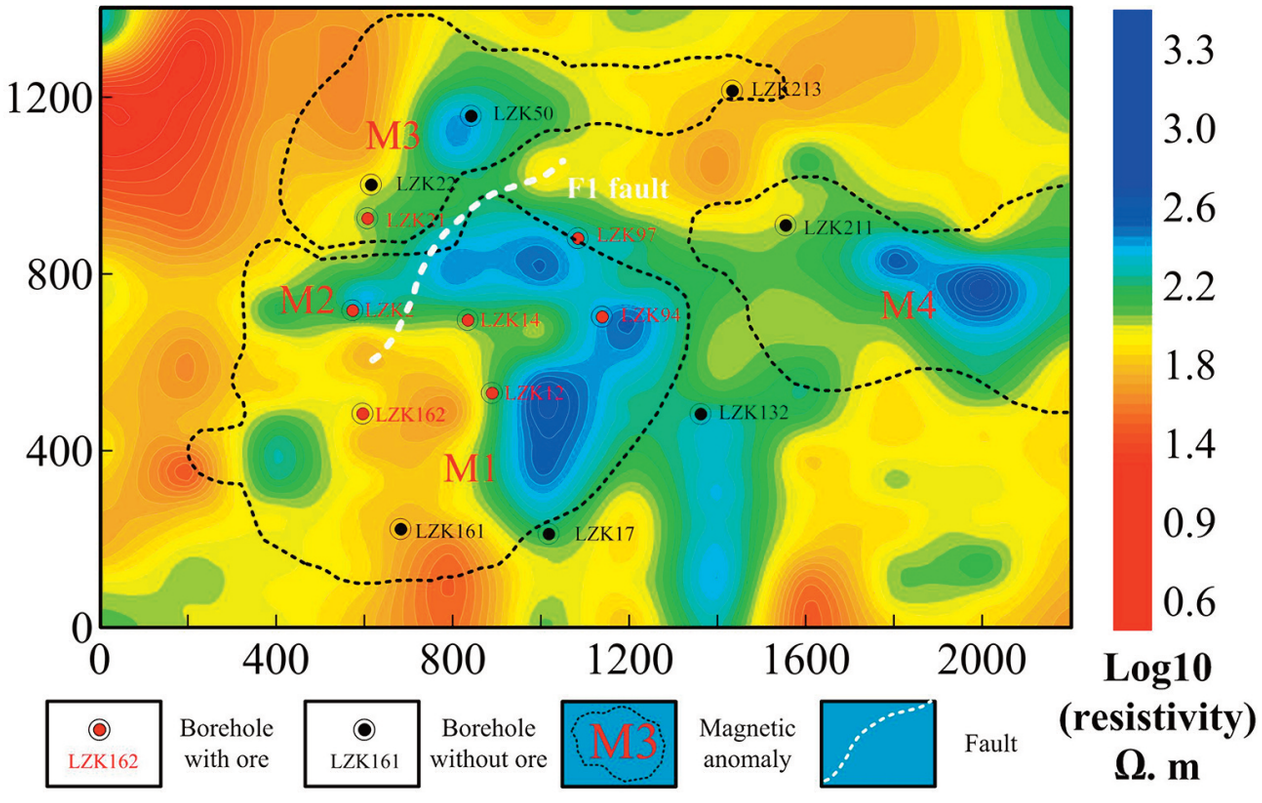

FIGURE 10. Resistivity slice map at a depth of 200 m of the Changyi BIF deposit superimposed with magnetic anomaly, boreholes, and fault location.

boreholes location. This is a typical positive and negative magnetic anomaly at ground surface produced by an approximately horizontal magnetic object present underground [Clark et al., 1994], consistent with the depositional mineralization of the survey area.

There are some high resistance regions in the middle and east of the survey area superimposed to on overall low resistivity background. The high resistance is inferred as the granite branches intrusion, uplift and deform the stratum of the survey area and affect the electrical and magnetic field distribution. It can be inferred that the slight positive magnetic anomaly M4 is related to granite intrusion, although there is uncertainty on relation between M4 and ore-body according to available information. How-

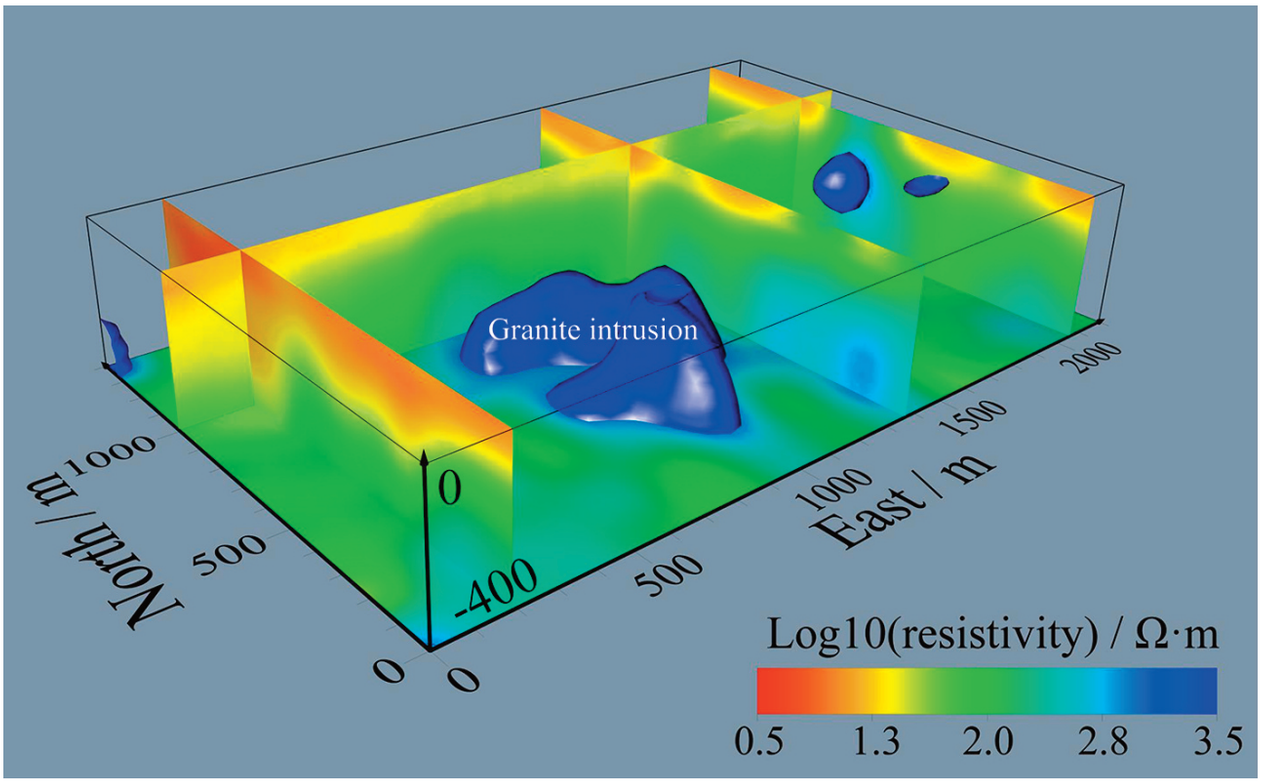

FIGURE 11. A three-dimensional display of Changyi BIF deposit intrusion between ground level to a depth of -400 m.

ever, there is no obvious influence on magnetic distribution of M1 and M2 since the magnetic anomaly aroused by the intrusion is smaller than that of the ore-body.

In order to visualize the intrusion intuitively, a three-dimensional model of granite intrusion is given in Figure 11. According to the regional geological data, the intrusion occurred after the depositional mineralization and led to the ore-body burial at a shallow depth and burial angle tilt. The ore-body status can be obtained indirectly by investigating the granite intrusion using resistivity data. Combined with magnetic data and other information, we can infer the spatial distribution of the ore-body.

6. CONCLUSION

The use of a new S-ATEM system based on an UHS is presented in this paper with an overview of the system and data processing technique. The S-ATEM system employs a grounded electrical source and a receiving unit with a lightweight design. A case study of an investigation performed using S-ATEM system in the Changyi BIF ore deposit is also illustrated. Results from the survey indicate that the S-ATEM system can provide an accurate estimation of the underground resistivity in case of areas with low resistivity and investigation depth not less than 400 m. The S-ATEM results have a good correspondence with a magnetic anomalies reconstructed with the ground magnetic method. Analysing the resistivity result in combination with other geo-information allows deducing information on the formation mechanism, distribution, and burial depth of the ore-body.

Results from the application of S-ATEM system proved that it can be used as a solution for resistivity investigation. The resistivity structure determined by S-ATEM survey is effective for basic data acquisition to predict ore-body distribution information in mineral exploration.

Acknowledgements. We acknowledge the reviewers and editors for their constructive remarks and suggestions. This research was supported by R&D of Key Instruments and Technologies for Deep Resources Prospecting (the National R&D Projects for Key Scientific Instruments), Grant No. ZDYZ2012-1-03-05.

REFERENCES

Abd Allah, S. et al. (2013). Three-dimensional resistivity characterization of a coastal area: Application of Grounded Electrical-Source Airborne Transient Electromagnetic (GREATEM) survey data from Ku-

jukuri Beach, Japan. Journal of Applied Geophysics, 99, 1–11.

Abd Allah, S. et al. (2014). Three-dimensional resistivity modelling of grounded electrical-source airborne transient electromagnetic (GREATEM) survey data from the Nojima Fault, Awaji Island, south-east Japan. Exploration Geophysics, 45, 49–61.

Bosschart, R. A. et al. (1972). Advances in deep penetration airborne electromagnetic methods. Conf. Proc. 24 International Geological Congress, section 9, 37-48.

Buselli, G. et al. (1996). Robust statistical methods for reducing sferics noise contaminating transient electromagnetic measurement. Geophysics, 61, 1633–1646.

Clark, D. A. et al. (1994). Iron: magnetic properties magnetic signatures of BIFs of the Hamersley Basin and Yilgarn Block, Western Australia. ASEG Extended Abstracts, 341-354.

Constable, S. C. et al. (1987). Occam's inversion: a practical algorithm for generating smooth models from EM sounding data. Geophysics , 52, 289-300.

Elliott, P. (1996). New airborne electromagnetic method provides fast deep-target data turnaround. The Leading Edge, 15(4), 309.

Elliott, P. (1998). The principles and practice of FLAIRTEM. Exploration Geophysics, 29, 58-60.

Fitterman, D. V. (2004). Effect of bird maneuver on frequency-domain helicopter EM response. Geophysics, 69(5), 1203-1215.

Fountain, D. K. (1998). Airborne electromagnetic systems - 50 years of development. Exploration Geophysics, 29(2), 1–11.

Ito, H. et al. (2014). Grounded electrical-source airborne transient electromagnetics (GREATEM) survey of Aso Volcano, Japan. Exploration Geophysics, 45, 43–48.

Ito, H. et al. (2011). Further investigations of underground resistivity structures in coastal areas using grounded source airborne electromagnetic. Earth, Planets, and Space, 63, e9–e12.

Liu, F. B. et al. (2017). Application of the EEMD method for distinction and suppression of motion-induced noise in grounded electrical source airborne TEM system. Journal of Applied Geophysics, 139, 109–116.

Lane, R. et al. (2000). An example of 3D conductivity mapping using the TEMPEST airborne electromagnetic system. Exploration Geophysics, 31, 162-172.

Lan, T. G. et al. (2012). Geological and geochemical characteristics of Paleoproterozoic Changyi banded iron formation deposit, Jiaodong Peninsula of eastern China. Acta Petrologica Sinica, 28(11),3595-3611 (in Chinese).

Mogi, T. et al. (1998). Development of Grounded Electrical Source Airborne Transient EM (GREATEM). Exploration Geophysics, 29, 61-64.

Mogi, T. et al. (2009). Grounded electrical-source airborne transient electromagnetic (GREATEM) survey of Mount Bandai, north-eastern Japan. Exploration Geophysics, 40, 1–7.

Macnae, J. C. et al. (1984). Noise processing techniques for time-domain EM system. Geophysics, 49, 934–948.

Munkholm, M. S. (1997). Motion-induced noise from vibration of moving TEM detector coil: cheracterisation and suppression. Journal of Applied Geophysics, 37, 21–29.

Nabighian, M. N. et al. (2005). Electrical and EM methods 1980-2005. The Leading Edge, 24, 42-45.

Okazaki, K. et al. (2011). Airborne electromagnetic and magnetic surveys for long tunnel construction design. Physics and Chemistry of the Earth, 36, 1237–1246.

Smith, R. S. et al. (2001). A comparison of data from airborne, semi-airborne, and ground electromagnetic systems. Geophysics, 66(5), 1379-1385.

Song, M. C. (2008). The composing, setting and evolution of tectonic units in Shandong Province. Geological Survey and Research, 31(3), 165-175 (in Chinese).

Wang, J. H. et al. (2014). Geology, deposit REE and trace elements characteristics of the Lianhuashan iron deposit in Changyi County, Shandong Province. ACTA PETROLOGICA ET MINERALOGICA, 33(2), 355- 364 (in Chinese).

Wang, S. T. et al. (2007). Geological characteristics of Neoproterozoic metamorphic sedimentary iron deposit in east part of Changyi area in Shandong Province. Shandong Land and Resources, 23(1), 45-48 (in Chinese).

Yin, C. C. et al. (2004). Attitude corrections of helicopter EM data using a superposed dipole model. Geophysics, 69(2), 431-439.

Zeng, G. X. et al. (1998). Shandong Iron Deposit[M]. Jinan: Shandong Science and Technology Press (in Chinese with English abstract).

Zhdanov, M. C. et al (2010). Electrical and Electromagnetic Methods. 53-8

*CORRESPONDING AUTHOR: Fubo LIU,
Key Laboratory of Electromagnetic Radiation and Sensing Technology
Institute of Electronics, Chinese Academy of Sciences,
Beijing, People's Republic of China

email: fbliu@mail.ie.ac.cn